Current Microbiology (2024) 81:100
https://doi.org/10.1007/s00284-024-03616-w

Green-Synthesized Silver Nanoparticles in the Prevention of Multidrug-Resistant *Proteus mirabilis* Infection and Incrustation of Urinary Catheters BioAgNPs Against *P. mirabilis* Infection

Gustavo Issamu Asai Saikawa[1] · Gustavo Henrique Migliorini Guidone[1] · Sandriele Aparecida Noriler[2] · Guilherme Fonseca Reis[2] · Admilton Gonçalves de Oliveira[2,3] · Gerson Nakazato[4] · Sergio Paulo Dejato Rocha[1]

Received: 31 January 2023 / Accepted: 10 January 2024 / Published online: 19 February 2024

Abstract

This study aimed to assess the activity of AgNPs biosynthesized by *Fusarium oxysporum* (bio-AgNPs) against multidrug-resistant uropathogenic *Proteus mirabilis*, and to assess the antibacterial activity of catheters coated with bio-AgNPs. Broth microdilution and time-kill kinetics assays were used to determine the antibacterial activity of bio-AgNPs. Catheters were coated with two (2C) and three (3C) bio-AgNPs layers using polydopamine as crosslinker. Catheters were challenged with urine inoculated with *P. mirabilis* to assess the anti-incrustation activity. MIC was found to be 62.5 µmol l-1, causing total loss of viability after 4 h and bio-AgNPs inhibited biofilm formation by 76.4%. Catheters 2C and 3C avoided incrustation for 13 and 20 days, respectively, and reduced biofilm formation by more than 98%, while the pristine catheter was encrusted on the first day. These results provide evidence for the use of bio-AgNPs as a potential alternative to combat of multidrug-resistant *P. mirabilis* infections.

Introduction

Urinary tract infections (UTIs) affect a significant number of individuals worldwide, with *Proteus mirabilis* being a common causative agent [1]. This microorganism is particularly associated with complicated UTIs, such as catheter-associated urinary tract infections (CAUTIs), which can lead to increased morbidity and mortality [1–3]. *P. mirabilis* produces potent urease, which hydrolyzes urea and contributes to the formation of crystals, including kidney stones, in the urinary tract [4]. These stones can cause severe complications, blockage of kidney ducts, and result in conditions like urosepsis [4]. Moreover, *P. mirabilis* can form crystalline biofilms that may incrust and block catheters, leading to further complications [2].

P. mirabilis developed resistance to several classes of antibiotics, complicating the treatment. In addition, the tendency of this organism to become encased in urinary calculi or within crystalline biofilms in urinary catheters can protect the bacteria and thus lead to treatment failures [3]. To address these issues, silver nanoparticles (AgNPs) have gained attention due to their antimicrobial properties. Manipulating the size of AgNPs at the nano-level enhances their antimicrobial effects, and they have demonstrated activity against multidrug-resistant Gram-positive and Gram-negative bacteria [5–8]. The exact mechanisms of AgNPs' antimicrobial action are not fully understood but are believed to be multifactorial.[7].

Synthesis of nanoparticles can be achieved via physical, chemical, and biological protocols. Biosynthesis, a form of green synthesis, has become increasingly prevalent because it is less expensive, produces stable nanoparticles, and uses mild reaction conditions [6]. Biosynthesis of metal nanoparticles exploits the molecular machinery that microorganisms use for detoxifying heavy metals [9]. Biomolecules produced

✉ Sergio Paulo Dejato Rocha
rochaspd@uel.br

1 Laboratory of Bacteriology, Department of Microbiology, Center of Biological Sciences, State University of Londrina, Rodovia Celso Garcia Cid PO-BOX 6001, Londrina 86051-980, Brazil

2 Laboratory of Microbial Biotechnology, Department of Microbiology, Center of Biological Sciences, State University of Londrina, Londrina, Brazil

3 Laboratory of Electron Microscopy and Microanalysis, State University of Londrina, Londrina, Brazil

4 Laboratory of Basic and Applied Bacteriology, Department of Microbiology, Center of Biological Sciences, State University of Londrina, Londrina, Brazil

by the microorganisms serve as reducing agents for metal ions and stabilizing agents as the bio-reduced metal atoms coalesce and form nanoparticles [10].

Surface modification has a central role in the functionality of biomaterials, such as catheters [11]; since bacteria need to adhere to a surface to form a biofilm, preventing this step may reduce the risk of infection. One method by which this can be achieved is through presentation of a bound antimicrobial agent on the bio-material surface [12]. Polydopamine (PDA) is used as a surface coating that serves to anchor antibacterial agents to biomaterials, producing an antimicrobial surface [13]. PDA can be applied as an aqueous solution onto virtually any solid substrate, inorganic or organic, including superhydrophobic surfaces, with controllable film thickness. It is durable and stable as a result of the self-polymerization properties of dopamine [14, 15]. The objective of this study was to produce a multilayered coating of green synthesized AgNPs using PDA as a crosslinker on urinary Foley catheters, and to assess the anti-incrustation and antibacterial activity of the AgNP layer against multidrug-resistant *P. mirabilis.*

Materials and Methods

Bacterial Isolate

Extended-spectrum *β*-lactamases (ESBL)-producing *P. mirabilis* LBUEL H54 was isolated from urine of a male patient hospitalized at Londrina University Hospital (Londrina, Paraná, Brazil) in 2015. The bacteria showed resistance to several antibiotics (amikacin, gentamicin, amoxicillin/clavulanic acid, ampicillin, aztreonam, cephalothin, cefuroxime, ceftazidime, ceftriaxone, cefepime, ciprofloxacin, norfloxacin, nalidixic acid, sulfamethoxazole/trimethoprim) and was used for all antibacterial assays. The isolate was identified and the antibiograms were determined using the Vitek® 2 Compact system (BioMérieux, Marcy-l'Etoile, France). Additionally, *P. mirabilis* specie also confirmed by biochemical screening by EPM, MiLI (PROBAC™, BR), Simmons citrate (Difco™, USA) and phenylalanine (Difco™, USA).

Fungal Isolate Identification and Taxonomic Description

F. oxysporum, strain 551, obtained from the culture collection of the Molecular Genetics Laboratory of ESALQ-USP (Piracicaba, São Paulo, Brazil), was used for AgNP synthesis. *F. oxysporum,* strain 551, is a non-pathogenic strain for humans, isolated from a soil collection, in the Atlantic Forest biome (Piracicaba, São Paulo, Brazil, 22°42′3"S 47°38′3 "W), collected on 03/01/2000.

The *F. oxysporum* strain 551 was characterized according to its macromorphological and micromorphological characteristics (ESM Fig. S1) according to previously described methodologies [16, 17]. Briefly, the fungal isolate was cultivated in PDA for 4 days at 28 °C, to analyze the macromorphological characteristics and micromorphologies of the vegetative and reproductive structures. Images of the fungal colony on the PDA were obtained. The structures were observed using a specific optical Olympus CX43 in bright field under 400×magnification. The images were generated using the Epview software.

For molecular characterization, the isolate 551 was grown on potato-dextrose broth (PDB) in shaker 150 rpm at 28 °C for 3 days, and the genomic DNA was extract according to protocol previously described [18]. For the phylogenetic analysis the ITS 5.8S region, partial of the elongation factor 1-alpha (*tef1*), and RNA polymerase second largest subunit gene (*rpb2*) genes were amplified and sequenced as described using primers ITS5 and ITS4 [19], EF1 & EF2 [20], RPB2-5f2 & RPB2-7cr [21], respectively, as recommended for *Fusarium* species [22]. Amplicons were obtained as described by Noriler et al. (2018) [23], using the same primer pairs as were used for amplification to ensure integrity of the sequences.

The curation of the chromatograms, sequences, alignment and substation model were performed as described by Noriler et al., (2019) [24]. The sequences used for performed the phylogenetic analysis were curated from the literature from the *Fusarium oxysporum* species complex (FOSC) [22, 25, 26]. Phylogenetic inference was based on Bayesian Inference (BI) using MrBayes version 3.2.1 [27].

The identification of the isolate 551 was based on phylogenetic analysis of the gene makers, comparing with other species from the FOSC described in the literature [22, 25, 26]. We could group the *Fusarium* isolate 551 in the FOSC group closest to *Fusarium fabacearum* (ESM Fig. S2), although the polytomy indicated that maybe more isolates from the species or even other genes are needed to solve the phylogenetic relationship between these strains. Moreover, as mentioned in the literature the FOSC is a highly diverse group, and much effort has been made to correctly characterize all the species inside this complex. The authors suggested that epitypification and neotypification of old names are still needed [26, 28].

Biosynthesis of AgNPs

Green-synthesized AgNPs (bio-AgNPs) were prepared following a previously described method [29]. Briefly, *F. oxysporum* was cultivated on malt agar (Acumedia®) with 0.5% (wt/v) yeast extract for 7 days at 28 °C. Fungal biomass was weighed, added to distilled water at a concentration of 0.1 g/ml^{-1}, and incubated for 72 h at 28 °C. The solution

was filtered and $AgNO_3$ (Merck™) was added to the filtrate at 10 mmol l^{-1} concentration. The solution was incubated for 15 days at 28 °C in the absence of light. Color change of the solution from pale yellow to dark brown was indicative of AgNP synthesis.

Characterization of Bio-AgNPs

The size distribution of the bio-AgNPs was determined by Photon Correlation Spectroscopy (PCS) and zeta potential was determined by Laser Doppler Electrophoresis (LDE) using a ZetaSizer NanoZS (Malvern Panalytical). The transmission electron microscopy (TEM) image to verify the shape of the Bio-AgNPs was obtained using the FEI Tecnai 12TM equipment. The BioAgNP sample was prepared with diluted deionized water and deposited on a Cu grid and dried at room temperature.

Antibacterial Activity of Bio-AgNPs

Broth Microdilution Assay

Broth microdilution assay was used to assess the minimal inhibitory concentration (MIC) according to Clinical and Laboratory Standards Institute guidelines [30]. Bio-AgNPs were tested at final concentrations ranging from 7.8 to 500 µmol l^{-1}. Sterile Mueller–Hinton broth (MHB, Difco™) was used as a negative control and MHB inoculated with *P. mirabilis* LBUEL-H54 was used as positive control. *P. mirabilis* LBUEL-H54 was stored in 25% glycerol (Merck™) at − 20 °C. Stored *P. mirabilis* LBUEL-H54 was incubated in MHB at 37 °C for 24 h and was tested at a final concentration of approximately 5×10^5 CFU/ml^{-1}. MIC was defined as the lowest concentration of bio-AgNPs able to inhibit the visible growth of *P. mirabilis* LBUEL-H54.

Time-Kill Assay

Time-kill assay was performed according to NCCLS (1999) [31]. *P. mirabilis* LBUEL-H54 was incubated in the presence of bio-AgNPs at the MIC, or absence of bio-AgNPs at 37 °C. Aliquots were taken in triplicate at 0, 15, 30 and 60 min, 2 h, 4 h, 8 h, 12 h, and 24 h and transferred to Mueller–Hinton agar (MHB, Difco™). CFU/ml^{-1} were counted to build a curve of $\log_{10}$ CFU/ml^{-1}/hour of exposure to the bio-AgNPs.

Antibiofilm Activity of Bio-AgNPs

XTT reduction assay was used to assess the inhibitory capacity of bioAgNPs against *P. mirabilis* LBUEL-H54 biofilm formation. XTT (2,3-bis (2- 161 methoxy-4-nitro-5-sulfophenyl)-2H-tetrazolium-5-carboxanilide) (Merck™) and menadione (Merck™) solutions were prepared as previously described [32]. Briefly, XTT solution was prepared in phosphate buffered saline (PBS, 10 mmol l^{-1}, pH 7.4) at a concentration of 1 mg/ml^{-1}, sterilized by filtration, and kept at − 20 °C. Menadione was prepared at 1 mmol l^{-1} in acetone, and a working solution of XTT/menadione (12.5:1 (v/v) was prepared.

100 µl *P. mirabilis* LBUEL-H54 (10^5 CFU/ml^{-1}) was incubated with bioAgNPs at MICs of 0.5, 1, and 2 in 96-well plates in quintuplicate for 24 h at 37 °C. After incubation, MHB was removed and wells were washed three times with PBS. 13.5 µl XTT/menadione solution in 100 µl of PBS was added to each well and incubated for 4 h at 37 °C in absence of light. Absorbance was read at 490 nm. The percentage of biofilm inhibition was calculated using the equation [(OD growth control—OD sample)/OD growth control]×100 [33]. *P. mirabilis* LBUEL-H54 culture in absence of bio-AgNPs served as a positive control and MHB plus bio-AgNPs served as a negative control.

Surface Modification

Surface modification of the 3-way latex silicone-coated Foley catheter (SOLIDOR®, No 24), two layers (2C) or 3 layers (3C) of bio-AgNPs, adapted from [34]. Sterile catheters were cut into 6-cm lengths and coated with PDA. The catheter segments were immersed in 10 ml of dopamine solution (2 mg/ml-1 dopamine hydrochloride; Sigma-Aldrich™) in 10 mmol l^{-1} Tris buffer (pH 8.5) at 22 °C for 24 h on a shaker platform at 250 rpm. The catheters were left to dry for 1 h in a laminar flow cabinet, then immersed in 10 ml of bio-AgNPs solution (10 mmol l^{-1}) and incubated for 24 h in a shaker at 250 rpm. The last step was repeated once for generation of 2C catheters and twice for generation for the 3C catheters.

Surface Characterization

2C and 3C catheters were subjected to energy dispersive X-ray spectroscopy (EDX) analysis. 1-cm pieces of catheters were analyzed in three distinct regions using two channels, from sodium to scandium and from titanium to uranium. Spectroscopy peaks were generated using Origin Pro 8 software (OriginLab).

Incrustation Assay

The incrustation assay was performed according to [34]. The capacity of 2C and 3C catheters to prevent incrustation was assessed by incubating 1-cm lengths of each catheter type in 2 ml of artificial urine (calcium chloride (0.049% wt/v), magnesium chloride hexahydrate (0.065% wt/v), sodium chloride (0.46% wt/v), di-sodium sulfate (0.23% wt/v), tri-sodium

citrate dehydrate (0.065% wt/v), di-sodium oxalate (0.002% wt/v), potassium dihydrogen phosphate (0.28% wt/v), potassium chloride (0.16% wt/v), ammonium chloride (0.1% wt/v), urea (2.5% wt/v), tryptic soy broth (0.1% wt/v), gelatin (0.5% wt/v)) inoculated with *P. mirabilis* LBUEL-H54 at a concentration of 10^5 CFU/ml^{-1}. The tubes were incubated at 37 °C with shaking at 100 rpm for 24 h. The catheter segments were transferred to a fresh inoculated artificial urine solution every 24 h. An uncoated catheter segment in artificial urine without bacteria served as a negative control and an uncoated, sterile catheter segment immersed in artificial urine with *P. mirabilis* LBUEL-H54 at (10^5 CFU/ml^{-1}) served as the positive control. Turbidity of the urine solution due to precipitate formation was used to indicate the onset of incrustation.

Antibiofilm Assay

1-cm lengths of 2C and 3C catheters were immersed in 2 ml of MHB with *P. mirabilis* LBUEL-H54 at a concentration of 10^5 CFU/ml^{-1} and incubated at 37 °C with shaking at 100 rpm for 24 h. A pristine catheter segment immersed in MHB with bacteria at the same concentration was used as a positive control, and a pristine catheter segment immersed in MHB without bacteria served as a negative control. The catheter segments were washed with saline solution (NaCl 0.9%) and treated with LIVE/DEAD™ BacLight™ L7007 (Invitrogen™). Bacterial viability (live bacteria stained green) was assessed by a confocal microscopy spectral (CMS) platform using a TCS SP8 microscope (Leica™).

Statistical Analysis

The experiments were performed in triplicate. Data were analyzed using the R software version 4.2.3. The Shapiro–Wilk test was used to verify the normality of the samples. To verify the independence of errors, the Durbin-Watson test was used. To analyze the Homoscedasticity of variances, the Lavene test was used. Analysis of variance (ANOVA) and Tukey post-test were performed. The results were considered statistically significant when $P < 0.01$.

Sequence Deposition

The DNA sequences of each region were deposited in the NCBI/GenBank with the accession numbers: OR853729 (ITS); OR865872 (*rpb2*); OR865873 (*tef1*).

Results

Characterization of Bio-AgNPs

TEM analysis showed that the bio-AgNP generated in this study were spherical (ESM Fig. S3). The average size of the bio-AgNPs, determined by PCS was 126.3 nm, and the average zeta potential, determined by LDE, was -36.86 mV (ESM Fig. S4).

Antibacterial Activity of Bio-AgNPs

Broth Microdilution Assay and Time-Kill Curve

The MIC of bio-AgNPs against *P. mirabilis* LBUEL-H54 was found to be 62.5 µmol l^{-1}. Temporal activity of AgNPs is shown in Fig. 1. The time to completely eliminate the number of viable cells is 4 h after starting the treatment. However, the reduction in the number of cells is already observed from the first minutes after treatment.

Antibiofilm Activity of Bio-AgNPs

XTT reduction assay was used to assess the metabolic activity of cells in the biofilm after 24 h of treatment with bio-AgNPs. At the MIC value, there was also a 76.4% reduction of biofilm formation, with similar results at supra-MIC treatment (76% reduction). However, treatment of biofilms

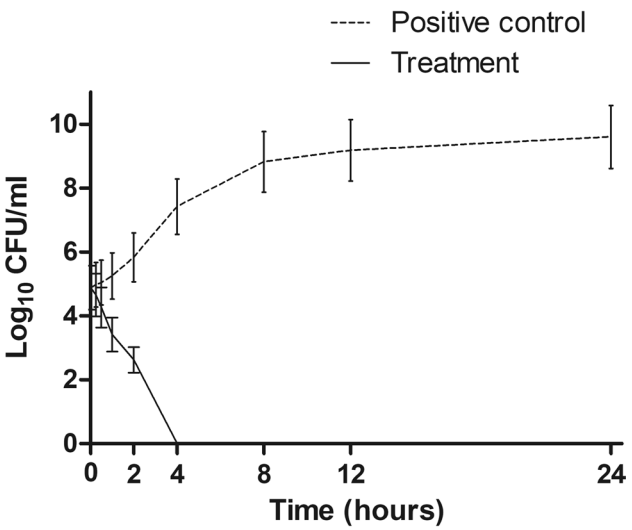

Fig. 1 Time-kill curve of AgNPs biosynthesized by *F. oxysporum* against *P. mirabilis* isolated from UTI. The time to completely eliminate the number of viable cells is 4 h after starting treatment. However, the reduction in the number of viable cells is visible after the first minutes of treatment. $P < 0.01$. Shapiro–Wilk statistical test and standard deviation of results

with sub-MIC resulted in an increase in biofilm formation when compared to the control. This result reveals the need to use doses above the MIC, thus avoiding inducing biofilm formation during possible treatments.

Surface Modification and Characterization of Catheter

As shown in Fig. 2, the surface of the catheter changed to a brownish color after the formation of the thin PDA film and to a dark brown after submersion in the bio-AgNP solution.

EDX analysis confirmed the presence of silver on the catheter (Fig. 3 and ESM Table S1). Silver was absent in the uncoated catheter but was present on catheter 2C and present at higher levels on catheter 3C, demonstrating that the multilayer coating strategy was successful and efficient, in addition to allowing manipulation of the amount of bio-AgNPs to be applied.

Incrustation Assay

Catheters 2C and 3C were challenged with artificial urine inoculated with 10^5 CFU/ml-1 *P. mirabilis* LBUEL-H54 to assess the capacity of inhibiting encrustation. After every 24 h, catheters were transferred to freshly prepared artificial urine. The turbidity of urine suggested encrustation as a result of precipitation of crystals [21]. Encrustation occurred right on the first day for the pristine catheter (Fig. 4). Catheter 2C was able to avoid encrustation for 13.5 ± 0.7 days and catheter 3C inhibited incrustation for 21 ± 1.4 days (ESM Fig. S5). Our data demonstrates that the greater the number of coating layers, the longer the time for incrustation to occur. Furthermore, there is a significant difference between the embedment time between the pristine catheter, the 2-layer coated catheter and the 3-layer coated catheter, $P < 0.01$.

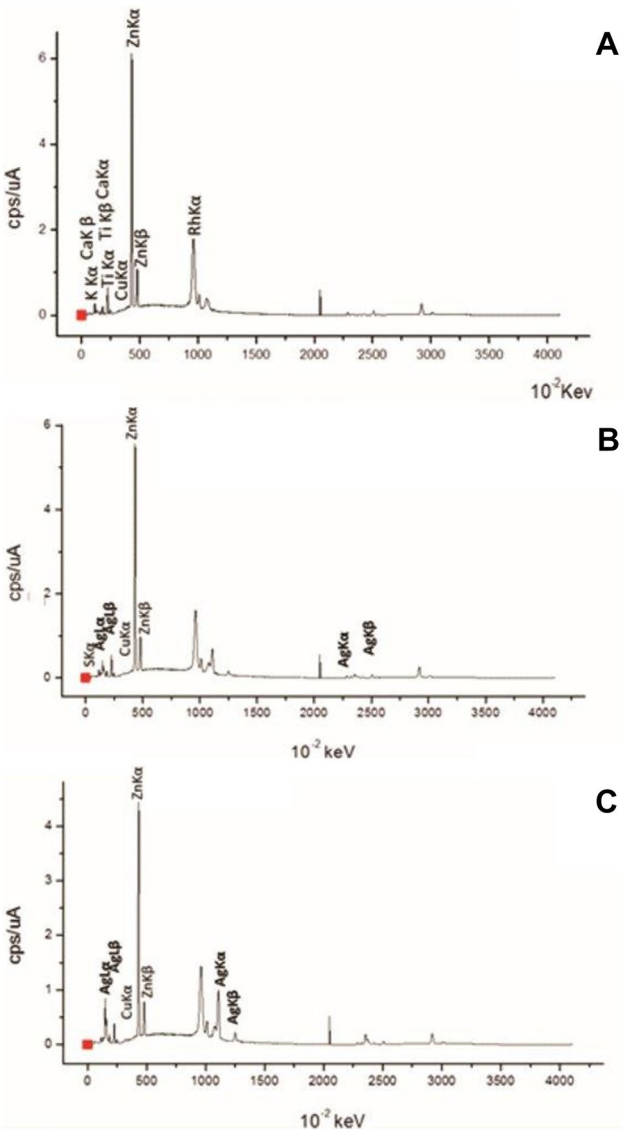

Fig. 3 EDX analysis of the surface of catheters. **A** Pristine catheter **B** Catheter 2C **C** Catheter 3C. The EDX analysis demonstrated the difference in Ag concentration between the different treatments. The pristine catheter did not show the presence of Ag. The 2-layer catheter showed 8.109 ± 2.7 and the 3-layer catheter 20.02 ± 3.6

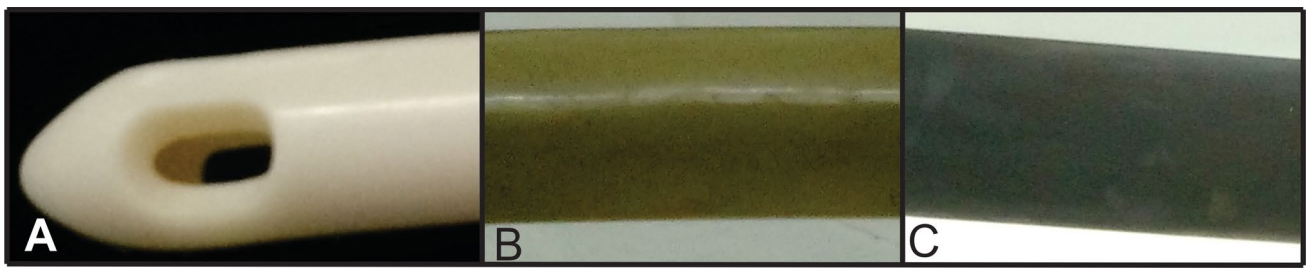

Fig. 2 Appearance of catheters. **A** pristine catheter **B** catheter coated with PDA **C** catheter coated with PDA + AgNPs. The change in color of the catheter with PDA indicates that there was polymerization and coating

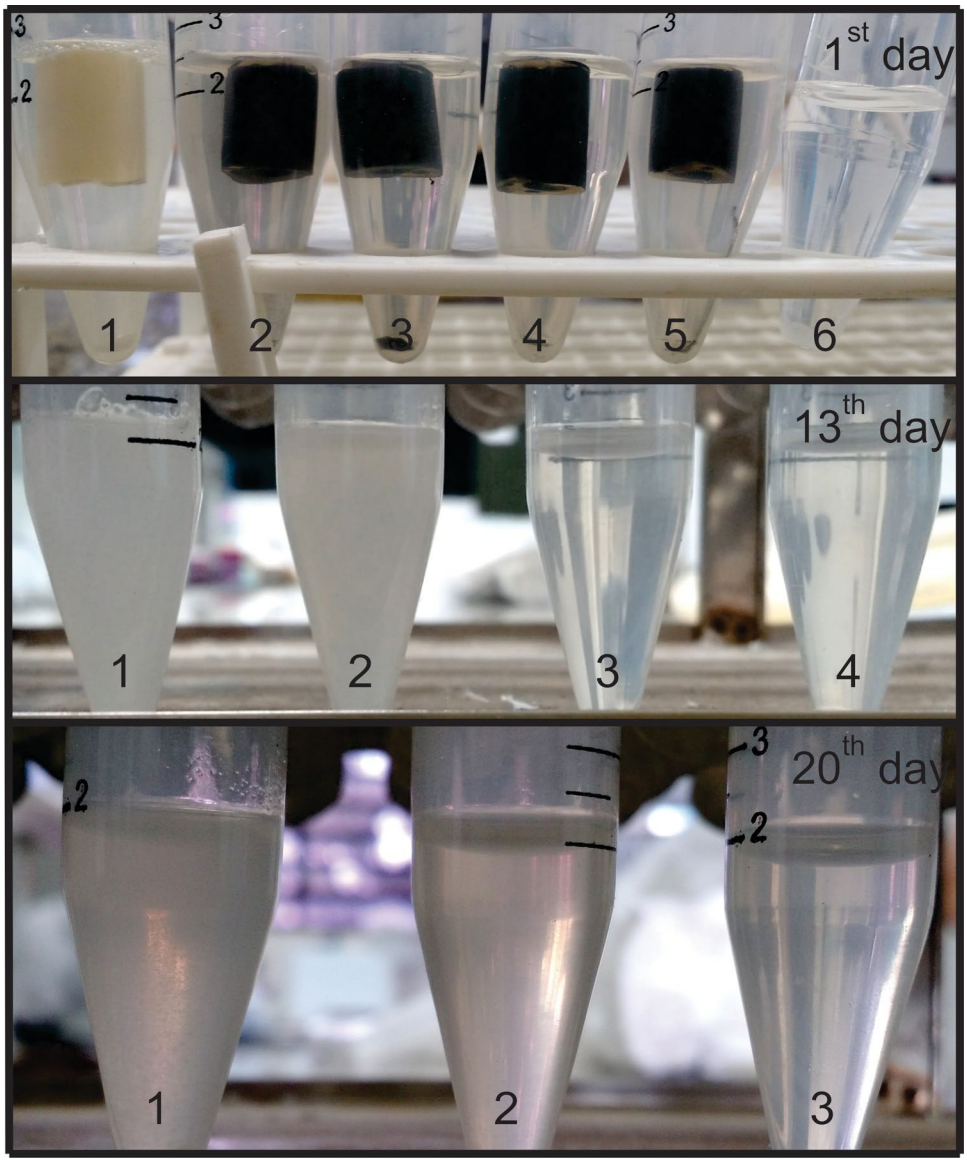

Fig. 4 Encrustation assay of catheters. 1st day: 1- positive control, 2- 2C, 3- 2C, 4- 3C, 5- 3C, 6- negative control. 13th day: 1- positive control, 2- 2C, 3- 3C, 4- negative control. 20th day: 1- positive control, 2- 3C, 3- negative control. The turbidity indicates the onset of encrustation

Antibiofilm Assay

The decrease in the number of viable bacteria in the 2C and 3C catheters compared to the uncoated control catheters was notable (Fig. 5). Fluorescence intensity measurements of viable bacteria on 2C catheters showed a 98.1% and 99.3% reduction on the external and luminal surfaces, respectively, compared to control catheters. Fluorescence analysis of viable bacteria in catheters 2C and 3C showed a reduction of 98.31% and 99.99% on the external and luminal surfaces, respectively ($P < 0.01$). These data demonstrate the efficiency of resurfacing with AgNPs against the present isolate, when compared with the untreated catheter.

Discussion

The morphology of bio-AgNPs generated in this study was shown to be spherical, consistent with reports of AgNPs synthesized using *F. oxysporum* found in literature [8, 29]. Studies have shown that the enzyme nitrate reductase is responsible for chemically reducing Ag + ions to AgNPs in *F. oxysporum*, and the isolated enzyme also produces spherical AgNPs [29, 35].

The antibacterial activity of AgNPs is size dependent [36]. The AgNPs synthesized by us had an average size of 126.3 nm and a MIC of 62.5 µmol l^{-1} (6.7 µg/ml-1) against uropathogenic *P. mirabilis* LBUEL-H54. However, the MIC value of AgNPs against *P. mirabilis* documented in the

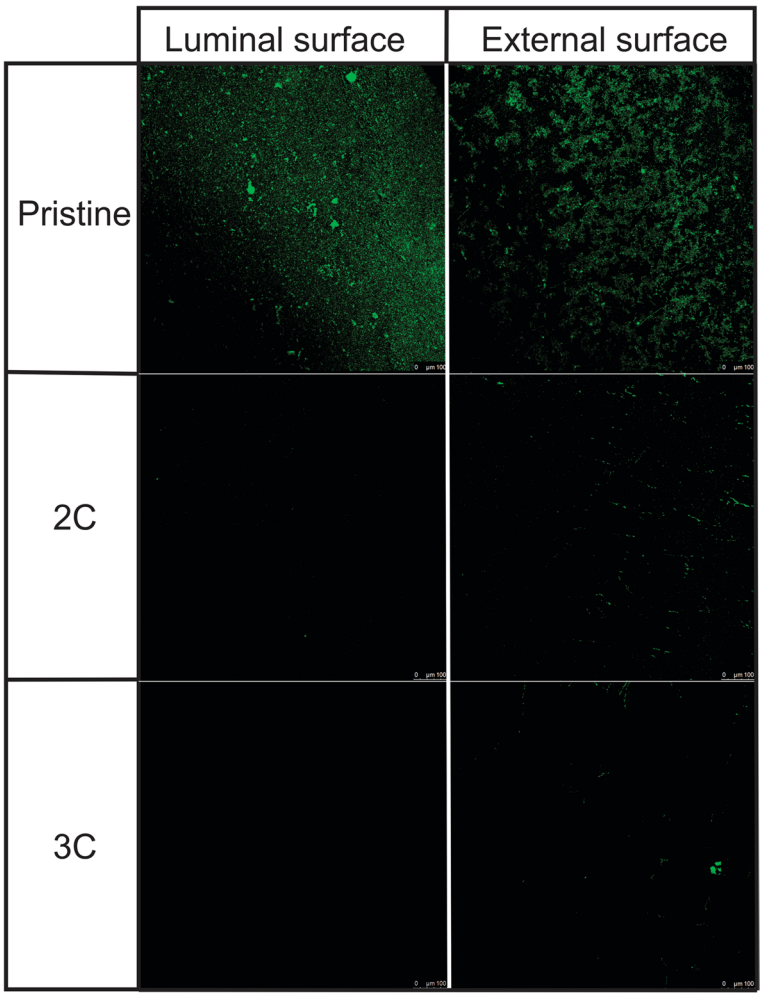

Fig. 5 Formation of biofilm by *P. mirabilis* on both luminal and external surfaces of catheters. The catheter treated 2C displayed a reduction of 98.1% on the external surface and 99.3% on the luminal surface. Similarly, the catheter treated 3C exhibited a reduction of 98.31% on the external surface and an impressive 99.99% on the luminal surface. The observations were made at 10×magnification, and the statistical analysis indicated significance at $P < 0.01$. Shapiro–Wilk statistical test

literature is variable [37, 38], with reports of AgNPs ranging from an average size of 10 nm and MIC of 150–250 µg/ml-1[39] to AgNPs with an average size of 16 nm and MIC of 2.5 µg/ml-1 [40]. Factors such as the AgNP features, bacterial strain, and methodologies applied can influence the antibacterial activity of AgNPs and might limit comparison between studies [10, 41].

According to the M26-A document [31], a bactericidal effect is a reduction ≥ 3log10 (99.9%) of the total count of CFU/ml-1. According to this definition, at MIC the bio-AgNPs in this study produced bactericidal activity at 2–4 h of treatment, as shown in Fig. 1. At the MIC value, there was also a 76.4% reduction of biofilm formation, with similar results at supra-MIC treatment (76% reduction). However, treatment of biofilms with sub-MIC resulted in an increase in biofilm formation when compared to the control. Stress response mechanisms, including high metal concentrations, are known to induce biofilm formation [42] and this may explain why, at sub-MIC, the presence of bio-AgNPs led to an increase in biofilm formation. Similarly, some antibiotics can induce biofilm formation at sub-inhibitory concentrations [43, 44]. Oxidative stress also can increase biofilm formation [45]. Given that an accepted mechanism for the antibacterial activity of AgNPs is the generation of reactive oxygen species [46], this also may also have contributed to the observed increase in biofilm formations at sub-MIC of bio-AgNP.

PDA has commonly been used to anchor biomolecules on biomaterial surfaces [11]. PDA has been also used to synthesize AgNPs insitu, acting directly as a reducing agent [34]. However, there is a lack of information about the antibacterial activity of the AgNPs produced without interfering substances such as PDA itself. Moreover, size characterization must usually be made by microscopy, a process which can change samples, create artifacts, and provides limited information about the size distribution and true population average of AgNPs [47, 48].

Our results show that AgNPs synthesized externally and properly characterized can be immobilized in the surface of the catheter using a PDA binding layer. Dopamine hydrochloride self-polymerizes in alkaline solutions, forming PDA [11]. A color change in the solution to dark brown

serves as the primary evidence for dopamine polymerization [49] and when applied to a surface, PDA forms a thin film [11]. As shown in Fig. 2, the surface of the catheter changed to a brownish color after the formation of the thin PDA film and to a dark brown after submersion in the bio-AgNP solution. EDX analysis confirmed the presence of silver on the catheter (Fig. 3 and ESM Table A1). Silver was absent in the uncoated catheter but was present on catheter 2C and present at higher levels on catheter 3C, demonstrating that the multilayer coating strategy was successful and allows for manipulation of the amount of bio-AgNPs to be applied.

P. mirabilis has been shown to be able to cause complete blockage of urine flow in catheters in less than 24 h [50]. In addition, commercially available catheters containing silver have not shown satisfactory performance. The Dover™ catheter inhibited incrustation for less than 7 days in experiments similar to those used in the present study [34]. The Bardex® I.C.™ catheter was completely blocked in 4.4 days in an in vitro study [51] and in 11 days in an in vivo study [52]. In a prospective, multicenter, nonrandomized, clinical study, Pickard et al. 2012 [53] concluded that the Bardex® I.C.™ catheter is not effective in reducing symptomatic CAUTI, suggesting that 1000 people would need to receive a silver alloy catheter to prevent one CAUTI, with the true effect lying between one infection prevented in 42 people and one infection caused in 45 people. Long-term catheterization is defined as a catheterization period $\geq$ 28 days [2]. However, infection and incrustation can occur Much sooner. Thus, the results obtained in the present study are particularly promising.

Both catheters 2C and 3C showed a notable performance in inhibiting biofilm formation, as indicated in Fig. 5. The analysis of intensity of fluorescence showed a reduction of 98.1% and 99.3% on fluorescence in external and luminal surfaces, respectively, in catheter 2C in comparison to the pristine catheter. Catheter 3C decreased the viability by 98.31% on the external surface and 99.99% on the luminal surface. These data provide evidence that coating with AgNPs can be effective against uropathogenic isolates of *P. mirabilis*.

Conclusion

In conclusion, this study is a demonstration of the efficacy of coating urinary catheters using a multilayer coating strategy, alternating between polydopamine and bio-AgNPS. Our results demonstrated that the AgNPs biosynthesized by *F. oxysporum* showed a significant capacity to inhibit the growth of planktonic cells of multiresistant *P. mirabilis*. Furthermore, the application of these nanoparticles in the urinary catheter enabled the inhibition of biofilm formation in cell culture. The bactericidal activity of bio-AgNPS is already known, making these substances possible alternative antimicrobials and with several proposed biotechnological activities. Thus, our proposal is a possible biotechnological application of these nanoparticles. However, it is important to highlight that further research and clinical studies are needed to fully validate the efficacy and safety of these nanoparticles in biomedical applications such as the one proposed in this study.

Supplementary Information The online version contains supplementary material available at https://doi.org/10.1007/s00284-024-03616-w.

Author Contributions All authors contributed to the study conception and design. GIAS, GHMG, SAN, GFR and AGOd: Material preparation, data collection and analysis were performed. AGdO, GN and SPDR: The first draft of the manuscript was written, and all authors commented on previous versions of the manuscript. All authors read and approved the final manuscript.

Funding This study was financed by the Coordination for the Improvement of Higher Education Personnel—Brazil (CAPES) Finance Code 001.

Data Availability Not applicable.

Code Availability Not applicable.

Declarations

Conflict of interest The authors declare that they have no known competing financial interests or personal relationships that could have appeared to influence the work reported in this paper.

Ethical Approval This study was performed in line with the principles of the Declaration of Helsinki. Approval was granted by the Ethics Committee of University State of Londrina (CEP-UEL 1.590.120).

Consent to Participate Informed consent was obtained from all individual participants included in the study.

Consent to Publication All authors listed in this manuscript provide their consent for publication of the research article.

References

1. Flores-Mireles AL, Walker JN, Caparon M, Hultgren SJ (2015) Urinary tract infections: epidemiology, mechanisms of infection and treatment options. Nat Rev Microbiol 13:269–284. https://doi.org/10.1038/nrmicro3432
2. Holling N, Lednor D, Tsang S et al (2014) Elucidating the genetic basis of crystalline biofilm formation in *Proteus mirabilis*. Infect Immun 82:1616–1626. https://doi.org/10.1128/IAI.01652-13
3. Schaffer JN, Pearson MM (2015) *Proteus mirabilis* and urinary tract infections. Microbiol Spectr. https://doi.org/10.1128/microbiolspec.UTI-0017-2013
4. Norsworthy AN, Pearson MM (2017) From catheter to kidney stone: the uropathogenic lifestyle of *Proteus mirabilis*. Trends Microbiol 25:304–315. https://doi.org/10.1016/j.tim.2016.11.015
5. Rai MK, Deshmukh SD, Ingle AP, Gade AK (2012) Silver nanoparticles: the powerful nanoweapon against multidrug-resistant bacteria: activity of silver nanoparticles against MDR bacteria.

J Appl Microbiol 112:841–852. https://doi.org/10.1111/j.1365-2672.2012.05253.x
6. Neethu S, Midhun SJ, Radhakrishnan EK, Jyothis M (2018) Green synthesized silver nanoparticles by marine endophytic fungus *Penicillium polonicum* and its antibacterial efficacy against biofilm forming, multidrug-resistant *Acinetobacter baumanii*. Microb Pathog 116:263–272. https://doi.org/10.1016/j.micpath.2018.01.033
7. Dakal TC, Kumar A, Majumdar RS, Yadav V (2016) Mechanistic basis of antimicrobial actions of silver nanoparticles. Front Microbiol. https://doi.org/10.3389/fmicb.2016.01831
8. Scandorieiro S, de Camargo LC, Lancheros CAC et al (2016) Synergistic and additive effect of oregano essential oil and biological silver nanoparticles against multidrug-resistant bacterial strains. Front Microbiol. https://doi.org/10.3389/fmicb.2016.00760
9. Park TJ, Lee KG, Lee SY (2016) Advances in microbial biosynthesis of metal nanoparticles. Appl Microbiol Biotechnol 100:521–534. https://doi.org/10.1007/s00253-015-6904-7
10. Durán N, Nakazato G, Seabra AB (2016) Antimicrobial activity of biogenic silver nanoparticles, and silver chloride nanoparticles: an overview and comments. Appl Microbiol Biotechnol 100:6555–6570. https://doi.org/10.1007/s00253-016-7657-7
11. Ding YH, Floren M, Tan W (2016) Mussel-inspired polydopamine for bio-surface functionalization. Biosurf Biotribol 2:121–136. https://doi.org/10.1016/j.bsbt.2016.11.001
12. Swartjes JJTM, Sharma PK, Kooten TG et al (2015) Current developments in antimicrobial surface coatings for biomedical applications. CMC 22:2116–2129. https://doi.org/10.2174/0929867322666140916121355
13. Su L, Yu Y, Zhao Y et al (2016) Strong antibacterial polydopamine coatings prepared by a shaking-assisted method. Sci Rep 6:24420. https://doi.org/10.1038/srep24420
14. Liu Y, Ai K, Lu L (2014) Polydopamine and its derivative materials: synthesis and promising applications in energy, environmental, and biomedical fields. Chem Rev 114:5057–5115. https://doi.org/10.1021/cr400407a
15. Zhou J, Xiong Q, Ma J et al (2016) Polydopamine-enabled approach toward tailored plasmonic nanogapped nanoparticles: from nanogap engineering to multifunctionality. ACS Nano 10:11066–11075. https://doi.org/10.1021/acsnano.6b05951
16. Fourie G, Steenkamp ET, Ploetz RC et al (2011) Current status of the taxonomic position of *Fusarium oxysporum* formae specialis cubense within the *Fusarium oxysporum* complex. Infect Genet Evol 11:533–542. https://doi.org/10.1016/j.meegid.2011.01.012
17. Khan MA, Khan SA, Waheed U et al (2021) Morphological and genetic characterization of *Fusarium oxysporum* and its management using weed extracts in cotton. J King Saud Univ - Sci 33:101299. https://doi.org/10.1016/j.jksus.2020.101299
18. Raeder U, Broda P (1985) Rapid preparation of DNA from filamentous fungi. Lett Appl Microbiol 1:17–20. https://doi.org/10.1111/j.1472-765X.1985.tb01479.x
19. White TJ, Bruns T, Lee S et al (1990) Amplification and direct sequencing of fungal ribosomal RNA genes for phylogenetics. PCR Protoc: Guide Methods Appl 18:315–322
20. O'Donnell K, Cigelnik E, Nirenberg HI (1998) Molecular systematics and phylogeography of the *Gibberella fujikuroi* species complex. Mycologia 90:465–493. https://doi.org/10.1080/00275514.1998.12026933
21. O'Donnell K, Gueidan C, Sink S et al (2009) A two-locus DNA sequence database for typing plant and human pathogens within the *Fusarium oxysporum* species complex. Fungal Genet Biol 46:936–948. https://doi.org/10.1016/j.fgb.2009.08.006
22. Lombard L, Sandoval-Denis M, Lamprecht SC, Crous PW (2019) Epitypification of *Fusarium oxysporum* – clearing the taxonomic chaos. Persoonia 43:1–47. https://doi.org/10.3767/persoonia.2019.43.01
23. Noriler SA, Savi DC, Aluizio R et al (2018) Bioprospecting and structure of fungal endophyte communities found in the brazilian biomes, pantanal, and cerrado. Front Microbiol 9:1526. https://doi.org/10.3389/fmicb.2018.01526
24. Noriler SA, Savi DC, Ponomareva LV et al (2019) Vochysiamides A and B: two new bioactive carboxamides produced by the new species diaporthe vochysiae. Fitoterapia 138:104273. https://doi.org/10.1016/j.fitote.2019.104273
25. Maryani N, Lombard L, Poerba YS et al (2019) Phylogeny and genetic diversity of the banana *Fusarium* wilt pathogen *Fusarium oxysporum f. sp. cubense* in the Indonesian centre of origin. Stud Mycol 92:155–194. https://doi.org/10.1016/j.simyco.2018.06.003
26. Wang MM, Crous PW, Sandoval-Denis M et al (2022) *Fusarium* and allied genera from China: species diversity and distribution. Persoonia 48:1–53. https://doi.org/10.3767/persoonia.2022.48.01
27. Ronquist F, Teslenko M, Van Der Mark P et al (2012) MrBayes 3.2: efficient bayesian phylogenetic inference and model choice across a large model space. Syst Biol 61:539–542. https://doi.org/10.1093/sysbio/sys029
28. Ariyawansa HA, Hawksworth DL, Hyde KD et al (2014) Epitypification and neotypification: guidelines with appropriate and inappropriate examples. Fungal Divers 69:57–91. https://doi.org/10.1007/s13225-014-0315-4
29. Durán N, Marcato PD, Alves OL et al (2005) Mechanistic aspects of biosynthesis of silver nanoparticles by several *Fusarium oxysporum* strains. J Nanobiotechnol 3:8. https://doi.org/10.1186/1477-3155-3-8
30. Clinical and Laboratory Standards Institute (2015) Methods for dilution antimicrobial susceptibility tests for bacteria that grow aerobically: M07-A10 ; approved standard, 10. ed. Committee for Clinical Laboratory Standards, Wayne, PA
31. Barry AL, Craig WA, Nadler H et al (1999) Methods for determining bactericidal activity of antimicrobial agents. Approv Guidel 19:1–3
32. Bazargani MM, Rohloff J (2016) Antibiofilm activity of essential oils and plant extracts against *Staphylococcus aureus* and *Escherichia coli* biofilms. Food Control 61:156–164. https://doi.org/10.1016/j.foodcont.2015.09.036
33. Chaieb K, Kouidhi B, Jrah H et al (2011) Antibacterial activity of thymoquinone, an active principle of Nigella sativa and its potency to prevent bacterial biofilm formation. BMC Complement Altern Med 11:29. https://doi.org/10.1186/1472-6882-11-29
34. Wang R, Neoh KG, Kang E et al (2015) Antifouling coating with controllable and sustained silver release for long-term inhibition of infection and encrustation in urinary catheters. J Biomed Mater Res 103:519–528. https://doi.org/10.1002/jbm.b.33230
35. Gholami-Shabani M, Akbarzadeh A, Norouzian D et al (2014) Antimicrobial activity and physical characterization of silver nanoparticles green synthesized using nitrate reductase from *Fusarium oxysporum*. Appl Biochem Biotechnol 172:4084–4098. https://doi.org/10.1007/s12010-014-0809-2
36. Raza M, Kanwal Z, Rauf A et al (2016) Size- and shape-dependent antibacterial studies of silver nanoparticles synthesized by wet chemical routes. Nanomaterials 6:74. https://doi.org/10.3390/nano6040074
37. Składanowski M, Golinska P, Rudnicka K et al (2016) Evaluation of cytotoxicity, immune compatibility and antibacterial activity of biogenic silver nanoparticles. Med Microbiol Immunol 205:603–613. https://doi.org/10.1007/s00430-016-0477-7
38. Srinivasan R, Vigneshwari L, Rajavel T et al (2018) Biogenic synthesis of silver nanoparticles using *Piper betle* aqueous extract and evaluation of its anti-quorum sensing and antibiofilm potential against uropathogens with cytotoxic effects: an in vitro and in vivo approach. Environ Sci Pollut Res 25:10538–10554. https://doi.org/10.1007/s11356-017-1049-0

39. Swarnavalli GCJ, Dinakaran S, Raman N et al (2017) Bio inspired synthesis of monodispersed silver nano particles using Sapindus emarginatus pericarp extract – Study of antibacterial efficacy. J Saudi Chem Soc 21:172–179. https://doi.org/10.1016/j.jscs.2015.03.004
40. Dhas SP, John SP, Mukherjee A, Chandrasekaran N (2014) Autocatalytic growth of biofunctionalized antibacterial silver nanoparticles: nanobiosynthesis of antibacterial AgNPs. Biotechnol Appl Biochem. https://doi.org/10.1002/bab.1161
41. Ruparelia JP, Chatterjee AK, Duttagupta SP, Mukherji S (2008) Strain specificity in antimicrobial activity of silver and copper nanoparticles. Acta Biomater 4:707–716. https://doi.org/10.1016/j.actbio.2007.11.006
42. Landini P (2009) Cross-talk mechanisms in biofilm formation and responses to environmental and physiological stress in *Escherichia coli*. Res Microbiol 160:259–266. https://doi.org/10.1016/j.resmic.2009.03.001
43. Hoffman LR, D'Argenio DA, MacCoss MJ et al (2005) Aminoglycoside antibiotics induce bacterial biofilm formation. Nature 436:1171–1175. https://doi.org/10.1038/nature03912
44. Aka ST, Haji SH (2015) Sub-MIC of antibiotics induced biofilm formation of *Pseudomonas aeruginosa* in the presence of chlorhexidine. Braz J Microbiol 46:149–154. https://doi.org/10.1590/S1517-838246120140218
45. Gambino M, Cappitelli F (2016) Mini-review: biofilm responses to oxidative stress. Biofouling 32:167–178. https://doi.org/10.1080/08927014.2015.1134515
46. Wang L, Hu C, Shao L (2017) The antimicrobial activity of nanoparticles: present situation and prospects for the future. IJN 12:1227–1249. https://doi.org/10.2147/IJN.S121956
47. Cho EJ, Holback H, Liu KC et al (2013) Nanoparticle characterization: state of the art, challenges, and emerging technologies. Mol Pharm 10:2093–2110. https://doi.org/10.1021/mp300697h
48. Bhatia S (2016) Natural Polymer Drug Delivery Systems. Springer International Publishing, Cham
49. Perikamana SKM, Shin YM, Lee JK et al (2017) Graded functionalization of biomaterial surfaces using mussel-inspired adhesive coating of polydopamine. Colloids Surf, B 159:546–556. https://doi.org/10.1016/j.colsurfb.2017.08.022
50. Milo S, Thet NT, Liu D et al (2016) An in-situ infection detection sensor coating for urinary catheters. Biosens Bioelectron 81:166–172. https://doi.org/10.1016/j.bios.2016.02.059
51. Rani SA, Celeri C, Najafi R et al (2016) Irrigation with N, N-dichloro-2,2-dimethyltaurine (NVC-422) in a citrate buffer maintains urinary catheter patency in vitro and prevents encrustation by *Proteus mirabili*s. Urolithiasis 44:247–256. https://doi.org/10.1007/s00240-015-0811-3
52. Morgan SD, Rigby D, Stickler DJ (2009) A study of the structure of the crystalline bacterial biofilms that can encrust and block silver Foley catheters. Urol Res 37:89–93. https://doi.org/10.1007/s00240-009-0176-6
53. Pickard R, Lam T, MacLennan G et al (2012) Antimicrobial catheters for reduction of symptomatic urinary tract infection in adults requiring short-term catheterisation in hospital: a multicentre randomised controlled trial. The Lancet 380:1927–1935. https://doi.org/10.1016/S0140-6736(12)61380-4